PFG NMR and Bayesian analysis to characterise non-Newtonian fluids

CrossMark

Thomas W. Blythe [a], Andrew J. Sederman [a,*], E. Hugh Stitt [b], Andrew P.E. York [c], Lynn F. Gladden [a]

[a] Magnetic Resonance Research Centre, Department of Chemical Engineering and Biotechnology, University of Cambridge, Pembroke Street, Cambridge CB2 3RA, UK
[b] Johnson Matthey Technology Centre, Billingham TS23 1LB, UK
[c] Johnson Matthey Technology Centre, Blounts Court, Sonning Common, Reading RG4 9NH, UK

ABSTRACT

Many industrial flow processes are sensitive to changes in the rheological behaviour of process fluids, and there therefore exists a need for methods that provide online, or inline, rheological characterisation necessary for process control and optimisation over timescales of minutes or less. Nuclear magnetic resonance (NMR) offers a non-invasive technique for this application, without limitation on optical opacity. We present a Bayesian analysis approach using pulsed field gradient (PFG) NMR to enable estimation of the rheological parameters of Herschel-Bulkley fluids in a pipe flow geometry, characterised by a flow behaviour index n, yield stress τ_0, and consistency factor k, by analysis of the signal in q-space. This approach eliminates the need for velocity image acquisition and expensive gradient hardware.

We investigate the robustness of the proposed Bayesian NMR approach to noisy data and reduced sampling using simulated NMR data and show that even with a signal-to-noise ratio (SNR) of 100, only 16 points are required to be sampled to provide rheological parameters accurate to within 2% of the ground truth. Experimental validation is provided through an experimental case study on Carbopol 940 solutions (model Herschel-Bulkley fluids) using PFG NMR at a ^1H resonance frequency of 85.2 MHz; for SNR > 1000, only 8 points are required to be sampled. This corresponds to a total acquisition time of <60 s and represents an 88% reduction in acquisition time when compared to MR flow imaging.

Comparison of the shear stress-shear rate relationship, quantified using Bayesian NMR, with non-Bayesian NMR methods demonstrates that the Bayesian NMR approach is in agreement with MR flow imaging to within the accuracy of the measurement. Furthermore, as we increase the concentration of Carbopol 940 we observe a change in rheological characteristics, probably due to shear history-dependent behaviour and the different geometries used. This behaviour highlights the need for online, or inline, rheological characterisation in industrial process applications.

1. Introduction

Many fluids encountered in everyday life, such as mayonnaise, toothpaste and shaving foam, exhibit both solid- and liquid-like behaviour. This non-Newtonian behaviour may be explained by considering the concept of yield stress, a parameter that quantifies the minimum shear stress that is required to be applied to a fluid before deformational flow can begin to occur. Fluids exhibiting yield stress behaviour demonstrate solid-like behaviour at low applied stresses, below the yield stress, but liquid-like behaviour at high applied stresses [1]. Although the existence of yield stress has been questioned [2,3], it nevertheless provides a convenient way for engineers to quantify (or predict) rheological behaviour.

For example, the rheological behaviour of many fluids can be accurately described using the Herschel-Bulkley constitutive equation:

$$\tau(\dot{\gamma}) = \tau_0 + k\dot{\gamma}^n, \tag{1}$$

where τ is shear stress, $\dot{\gamma}$ is shear rate, τ_0 is the yield stress of the fluid, and k and n represent the consistency factor and flow behaviour index, respectively. The relationship between τ and $\dot{\gamma}$, i.e. the flow curve $\tau(\dot{\gamma})$, can then be described conveniently using only rheological parameters appropriate to the Herschel-Bulkley constitutive equation. However, a major weakness of the Herschel-Bulkley constitutive equation is its inability to unambiguously establish the rheological parameters, since different sets of these parameters can provide equivalent fits to the experimental data [4].

Yield stress behaviour can be affected by changes in sample pH and concentration [5], with such properties responsible for changes in the flow curve. This can be detrimental to many industrial processes, particularly those involving flow [6]. The

characterisation and monitoring of the flow curve of fluids in these applications is therefore critical for process control and optimisation. In some cases, however, the flow curve is no longer a measure of the material properties of the fluid but depends on the shear history [1,7,8]. For this reason, rheological characterisation should be performed online, or inline, and in real-time, with the use of offline techniques, e.g. conventional benchtop rheometry methods [9], unsuitable for this application. Furthermore, there exists a need to obtain detailed information about the flow field generated by the device inducing deformational flow [10] to enable the observation and quantification of flow phenomena, including wall slip [9,11]. Whilst optical methods such as laser Doppler [12] and ultrasound velocimetry [13] enable the visualisation of the flow field, both involve tracer particles and are limited in the sample geometries that can be used. Light scattering techniques are also limited to optically transparent or semi-transparent fluid flows. In contrast, nuclear magnetic resonance (NMR) enables the non-invasive study of translational motion without limitation on optical opacity.

The study of translational motion using NMR was first realised by Carr and Purcell [14] through the exploitation of the sensitivity of spin-spin relaxation times. This has since developed, with phase encoding NMR techniques now widely considered to be the most robust and quantitative way of measuring flow [15]. Such techniques are often coupled with magnetic resonance (MR) imaging hardware, in a method termed MR flow imaging [16], to permit spatially resolved measurements of velocity in one, two, or three spatial dimensions. Arola et al. [17–19] used one-dimensional (1D) measurements of velocity to quantify fluid displacement as a function of radial position in a cylindrical pipe for non-Newtonian fluids demonstrating power-law [17,18] and Herschel-Bulkley [19] rheological behaviour. A pipe flow geometry is ideally suited to online, or inline, application. Shear rate data were evaluated through the linear least squares (LLS) regression of an even-order polynomial to the displacement data, followed by differentiation of the regression data. Measurements of pressure drop per unit length, dP/dL, were then used to quantify the shear stress at the wall, τ_w, using the following equation:

$$\tau_w = \frac{dP}{dL}\frac{R}{2},\tag{2}$$

which is derived from a force balance and where R represents the pipe radius. From Eq. (2) it can be shown that:

$$\tau = \frac{r}{R}\tau_w,\tag{3}$$

with r the radial position. Note that τ increases linearly from 0 at the centre of the pipe to τ_w at the wall and is independent of the rheological behaviour of the fluid under study. Using this approach, it is possible to characterise the flow curve over a range of shear rates in only a single measurement. A regression of a constitutive equation, such as Eq. (1), to the experimental flow curve may then be performed to provide estimates of the rheological parameters. The accuracy of this approach is sensitive to the accuracy of the pressure drop and displacement data obtained, therefore demanding adequate spatial and velocity resolution [17–19]. Arola et al. [19] suggest that over 100 spatially resolved velocity data points may be required to achieve an error in τ_0 of less than 2% when compared with conventional rheometry methods. Although a number of fast imaging sequences exist [20–22], many of these are unable to provide the spatial and/or temporal resolution required to ensure accurate rheological characterisation in real-time, and so the online, or inline, use of MR flow imaging in this application is challenging. By using the PFG method introduced in this work, MR rheometry is extended to single-axis gradient hardware, thereby eliminating the requirement of spatial encoding and enabling a substantial

reduction in data acquisition times such that online, or inline, measurements are now possible. This has potential for use in process control and optimisation. The principles underlying the developments presented in this work are now introduced.

For fluids demonstrating Herschel-Bulkley rheological behaviour, Eqs. (1) and (3) can be used to show that fluid displacement, ζ, in a cylindrical pipe flow geometry is described as a function of r by:

$$\zeta(r,n,r_0) = \begin{cases} \zeta_{max} & 0 \leqslant r < r_0, \\ \zeta_{max}\left(1 - \left(\frac{r-r_0}{R-r_0}\right)^{\frac{n+1}{n}}\right) & r_0 \leqslant r \leqslant R, \end{cases}\tag{4}$$

where ζ_{max} is the maximum fluid displacement. Fig. 1 shows displacement profiles obtained using Eq. (4) for three example fluids demonstrating Newtonian and non-Newtonian behaviour; $n = 1.0$ and $r_0/R = 0.0$, $n = 0.5$ and $r_0/R = 0.5$, and $n = 0.5$ and $r_0/R = 0.8$. It is seen in Fig. 1 that, for a fluid demonstrating Herschel-Bulkley rheological behaviour, there exists a plug flow region at the centre of the pipe bounded by r_0 and determined by evaluating Eq. (3) at $\tau = \tau_0$; within this plug flow region, $\tau \leqslant \tau_0$ and $\dot{\gamma} = 0\ s^{-1}$. Fluid displacement within the region bounded by r_0 and R increases from 0 at R to ζ_{max} at r_0. An increase in r_0 is responsible for an increase in the width of the plug flow region, a flattening of the displacement profile and a reduction in ζ_{max}. Similar trends are observed for a decrease in n. Changes in the rheological parameters of the fluid under study are, therefore, expected to induce changes in the displacement profiles and associated volume-averaged displacement probability distributions, or flow propagators [23]. Flow propagators completely characterise the flow under study [24] and are obtained through Fourier transform of the PFG NMR signal sampled in q-space, $S(q)$:

$$S(q) = \int p(\zeta)e^{i2\pi q\zeta}d\zeta,\tag{5}$$

where $p(\zeta)$ defines the flow propagator in terms of ζ and $q = (1/2\pi)\gamma g\delta$, with γ the gyromagnetic ratio of the nucleus under study and g and δ the magnitude and duration of the flow encoding gradient, respectively [25]. By controlling g it is possible to traverse q-space, with the field-of-flow (FOF) defined by the reciprocal of the sampling resolution in q-space and the velocity resolution of the flow propagator defined by the reciprocal of the range of q-space sampled. The signal acquired in q-space and the flow propagator represent mutually conjugate Fourier pairs, and so Fourier transform of $S(q)$ provides $p(\zeta)$ representative of the flow under study.
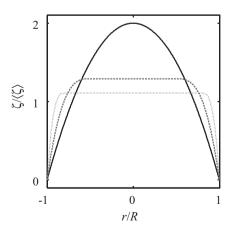

Fig. 1. Displacement profiles generated using Eq. (4) for three example fluids; with (—) $n = 1.0$ and $r_0/R = 0.0$, (——) $n = 0.5$ and $r_0/R = 0.5$, and (·····) $n = 0.5$ and $r_0/R = 0.8$. Fluid displacement and radial position are represented as a fraction of the mean fluid displacement and pipe radius, respectively.

The use of flow propagators for rheological characterisation was first proposed theoretically by McCarthy et al. [26], with $p(\zeta)$ defined by the rheological parameters of the fluid under study [27]. Whilst differences in the shape of the flow propagator have been reported for a range of Newtonian and non-Newtonian fluids [28], the quantitative use of flow propagators in this application remains challenging due to hardware limitations, i.e. gradient hardware, and practical constraints, such as data acquisition times, that limit the range of q-space accessible. The signal sampled at the limits of q-space will often not approach zero, and so the introduction of truncation artefacts into the flow propagator during Fourier transform may also be experimentally unavoidable. To this end, Blythe et al. [27] have recently exploited the sensitivity of $S(q)$ to changes in $p(\zeta)$ to enable the direct analysis of acquisition data, using cumulant analysis, thus removing the need for Fourier transform and preventing the introduction of truncation artefacts. Furthermore, strict sampling requirements are removed, allowing considerable reductions in acquisition times. This method was successfully applied to estimate n describing several power-law fluids. However, these measurements cannot be used for the unambiguous estimation of n, τ_0, and k describing Herschel-Bulkley fluids due to the known interdependence between n, τ_0, and k [29].

In this work, a Bayesian NMR approach is developed which estimates n, τ_0 and k, i.e. the flow curve, describing Herschel-Bulkley fluids. Furthermore, we show that these measurements can be achieved in as little as 60 s. We systematically investigate the robustness of our proposed Bayesian NMR approach to reduced sampling and noisy data using data generated through numerical simulations to determine the minimum number of data points needed to characterise the rheology with reasonable accuracy, here defined as ±5%, this error being typical of conventional rheometry methods [9]. Also considered is the sensitivity of the Bayesian NMR approach to changes in n and r_0/R of the flow under study. The results of the simulations are validated through an experimental study of model Herschel-Bulkley fluids, namely Carbopol 940 solutions [30,31], flowing within a cylindrical pipe. The rheological parameters and flow curves obtained using the Bayesian NMR approach are then compared with the same data obtained from MR flow imaging and conventional rheometry methods.

2. Model development

Bayesian analysis is a probabilistic method that has previously been applied in a variety of NMR applications [32–38]; it has been shown to improve the accuracy of flow measurements by the use of reduced sampling [33], and to enable the recovery of NMR spectra [32] and particle size distributions [37] from noisy data. In Bayesian analysis, the state of the system, θ, is inferred from a set of experimental measurements, $\hat{y}$, using the posterior probability density function, $p(\theta|\hat{y})$:

$$p(\theta|\hat{y}) \propto p(\hat{y}|\theta)p(\theta), \tag{6}$$

where $p(\hat{y}|\theta)$ is the likelihood function and $p(\theta)$ incorporates prior knowledge. In this work we extend current methodologies to enable the estimation of Herschel-Bulkley rheological parameters using PFG NMR, where $\hat{y}$ corresponds to the measured signal in q-space, $S(q)$, and θ corresponds to n and r_0/R describing the flow under study. Note that, in accordance with Eq. (3), τ_0/τ_w and r_0/R are interchangeable, thus enabling the estimation of τ_0 if τ_w is known. The likelihood function then describes the variation in $S(q)$ for a particular combination of n and r_0/R, and the prior describes what we already know about the probabilities of the values of n and r_0/R. A prior in which the probabilities within a specified range are identical is known as a simple uninformative prior. The

development of a Bayesian NMR approach enabling the estimation of these parameters is illustrated in Fig. 2 and will now be outlined.

The signal in q-space, $S(q)$, is measured in quadrature in the presence of Gaussian noise such that the likelihood function, $p(S(q)|n, r_0)$, takes the form:

$$p(S(q)|n, r_0) = \frac{1}{\sigma\sqrt{2\pi}} e^{-\frac{(|S(q)-f(q,n,r_0)|)^2}{2\sigma^2}}, \tag{7}$$

for flow that is stable over the experimental duration, i.e. laminar flow, and where $f(q, n, r_0)$ is the expected complex signal in q-space for a particular n and r_0/R, and σ is the standard deviation of the Gaussian noise in the real and imaginary channels. Here, σ is obtained from the experimental dataset. In addition to a variation of the phase of $S(q)$ and $f(q, n, r_0)$ with q, $S(q)$ may possess an additional phase offset due to the receiver. A comparison between $S(q)$ and $f(q, n, r_0)$ requires this phase offset be removed through the phase correction of $S(q)$, such that the phase of the signal at the centre of q-space is zero.

In order to determine $p(S(q)|n, r_0)$, we must first obtain $f(q, n, r_0)$ numerically. It is known from Eq. (5) that $S(q)$ is given by the Fourier transform of $p(\zeta)$. An analytical expression defining $p(\zeta)$ in terms of n and r_0/R in the absence of self-diffusion has previously been derived [39]:

$$p(\zeta, n, r_0) = \begin{cases} \frac{2}{\zeta_{max}} \frac{(R-r_0)}{R^2} \frac{n}{n+1} \left(1 - \frac{\zeta}{\zeta_{max}}\right)^{\frac{-1}{n+1}} \left(r_0 + (R-r_0)\left(1 - \frac{\zeta}{\zeta_{max}}\right)^{\frac{n}{n+1}}\right) & 0 < \zeta < \zeta_{max}, \\ \left(\frac{r_0}{R}\right)^2 \delta_{\zeta-\zeta_{max}} & \zeta = \zeta_{max}, \end{cases} \tag{8}$$

where ζ_{max} represents the maximum fluid displacement and $\delta_{\zeta-\zeta_{max}}$ is a Dirac delta function with respect to the displacement. Experimentally, an outflow of spins will lead to some loss of signal, with the amount lost proportional to the local displacement. To account for this, the following correction is applied to $p(\zeta, n, r_0)$ calculated using Eq. (8):

$$p'(\zeta, n, r_0) = (1 - \alpha)p(\zeta, n, r_0), \tag{9}$$

where $p'(\zeta, n, r_0)$ represents the experimentally acquired flow propagator and $\alpha = \zeta/L$, with L the length of the excitation region as determined by the experimental set-up. Further, self-diffusion
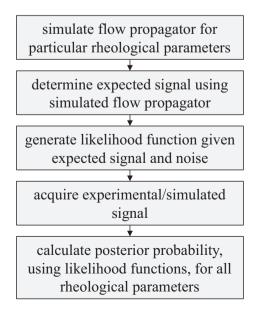

Fig. 2. Block diagram outlining the key stages in the proposed Bayesian NMR approach.

[25] is responsible for the Gaussian broadening of $p'(\zeta, n, r_0)$ such that the expected complex signal in q-space becomes:

$$f(q, n, r_0) = \frac{S(q, n, r_0)}{|S(0)|} = \int p'(\zeta, n, r_0) e^{i2\pi q \zeta - 4\pi^2 D(\Delta - \frac{\delta}{3})q^2} d\zeta, \quad (10)$$

where D is the diffusion coefficient and Δ the observation time. Fig. 3 shows (a) $p'(\zeta)$ and (b) the real component of $f(q)$, $\mathrm{Re}(f(q))$, for the three example fluids considered in Fig. 1. It is observed in Fig. 3(a) that a reduction in n and an increase in r_0/R, i.e. increase in τ_0/τ_w, causes a reduction in $\zeta_{\max}$ and an increase in the maximum probability. As shown in Fig. 3(b), the reduction in n and increase in r_0/R shown in Fig. 3(a) cause a reduction in the frequency of oscillations in $f(q)$ and an increase in $|f(q)|$ at the limits of q-space sampled. It is also interesting to note that, as follows from simple Fourier theory, the size of the plug flow region can be obtained from the magnitude of the signal at high-q if the diffusion coefficient is known, and its displacement can be obtained from the frequency of the oscillations in q-space. The expected signal is plotted across a q-space range of $\pm 2000 \text{ m}^{-1}$, with this corresponding to the optimum sampling range, determined to be $\pm 4 \langle \zeta \rangle^{-1} \text{ m}^{-1}$, where $\langle \zeta \rangle$ is the mean fluid displacement. The minimum number of q-space data points required to be sampled across this range is investigated in Section 3.1.

The simulation of $p'(\zeta, n, r_0)$ and thus $f(q, n, r_0)$ requires knowledge of $\zeta_{\max}$ which can only be determined if $\langle \zeta \rangle$ is known. When a comparison between $S(q)$ and $f(q, n, r_0)$ is required, accurate estimation of $\langle \zeta \rangle$ is achieved through measurement of the evolution of the phase of $S(q)$ at low values of q, where the measured phase shift is directly proportional to $\langle \zeta \rangle$. The integration of Eq. (4) with respect to the cross-sectional area of the pipe, and between the limits of 0 and R, gives the following expression:

$$\langle \zeta \rangle = \zeta_{\max} \left(\frac{n+1}{3n+1} + \frac{2r_0 n(n+1)}{R(2n+1)(3n+1)} + \frac{2n^2 r_0^2}{R^2(2n+1)(3n+1)} \right), \quad (11)$$

which can be used to calculate $\zeta_{\max}$ for a particular n and r_0/R. Flow propagators generated using Eqs. (8), (9) and (11) can therefore be used together with Eq. (10) to generate $f(q, n, r_0)$ for any combination of n and r_0/R. A 3D dictionary of f is constructed for all required n, r_0/R, and q, with the posterior probability of a particular n and r_0/R obtained from a set of experimental measurements of $S(q)$ by calculating the probability of each measurement using Eq. (7). The product of the individual probabilities gives the posterior probability of a particular n and r_0/R, as described by:

$$p(n, r_0 | \hat{y}) = \prod_{i=1}^{N} \frac{1}{\sigma \sqrt{2\pi}} e^{-\frac{(|S(q_i) - f(q_i, n, r_0)|)^2}{2\sigma^2}}, \quad (12)$$

where N is the number of sampled q-space data points. This is repeated for all combinations of n and r_0/R to quantify the full 2D posterior probability distribution, $p(\theta | \hat{y})$, where $\hat{y} = S(q)$ and $\theta = \{n, r_0\}$. The generation of $p(\theta | \hat{y})$ is summarised in Fig. 4. A summation of $p(\theta | \hat{y})$ along the r_0 and n axes may then be used to characterise $p(n | \hat{y})$ and $p(r_0 | \hat{y})$, respectively, with estimates of n and r_0/R given by the mean of these distributions and the standard deviation a measure of the uncertainty.

A corresponding measurement of dP/dL can then be used to estimate τ_0, according to Eqs. (2) and (3) where $\tau_0 = r_0 dP/(2dL)$, with an estimate of k given by [40]:

$$\frac{dP}{dL} = \frac{2k}{R} \left(\frac{\langle \zeta \rangle}{\Delta R} \right)^n \left(\frac{3n+1}{n} \right)^n \frac{1}{1-X} \left(\frac{1}{1 - aX - bX^2 - cX^3} \right)^n, \quad (13)$$

where

$$X = \frac{r_0}{R}, \quad (14)$$

$$a = \frac{1}{(2n+1)}, \quad (15)$$

$$b = \frac{2n}{(n+1)(2n+1)}, \quad (16)$$

$$c = \frac{2n^2}{(n+1)(2n+1)}. \quad (17)$$

Alternatively, a full 3D posterior probability distribution may be quantified using Eqs. (13)–(17), with a corresponding measurement of dP/dL (or distribution thereof) and $p(\theta | \hat{y})$, to estimate k for all combinations of n and τ_0. Complete rheological characterisation is therefore possible using the proposed Bayesian NMR approach, thus enabling the measurement of the flow curve over a range of shear rates in only a single measurement. Furthermore, the Bayesian NMR approach is applicable to single-axis gradient hardware and eliminates the need for Fourier transform, offering advantages over alternative techniques for the estimation of rheological parameters.
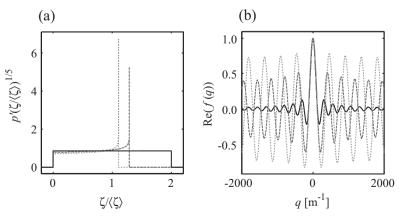

Fig. 3. (a) Flow propagators and (b) the corresponding real component of the expected signal in q-space, $\mathrm{Re}(f(q))$, across a range of $\pm 2000 \text{ m}^{-1}$ for three example fluids; with (——) $n = 1.0$ and $r_0/R = 0.0$, (– –) $n = 0.5$ and $r_0/R = 0.5$, and (···) $n = 0.5$ and $r_0/R = 0.8$. The expected signal was simulated with $\langle \zeta \rangle = 2$ mm in the absence of self-diffusion and an outflow of spins. The flow propagators have been scaled to the power of the fifth root to plot the entire plug flow region.
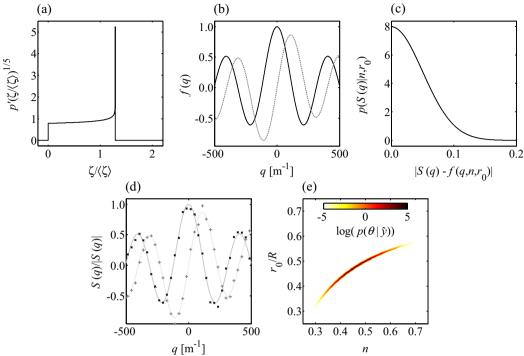
Fig. 4. A schematic to show the proposed Bayesian NMR approach: (a) $p'(\zeta)$ is simulated for a particular combination of n and r_0/R using Eqs. (8), (9) and (11); (b) Eq. (10) is used with $p'(\zeta)$ to calculate the expected signal in q-space, $f(q)$, for n and r_0/R, showing the (━) real and (╍) imaginary components of $f(q)$; (c) a likelihood function is generated using Eq. (7) through the addition of pseudo-random Gaussian noise to the real and imaginary channels of $f(q)$; (d) the required points in q-space are sampled experimentally, showing the ($\times$) real and ($+$) imaginary components of $S(q)$; (e) the posterior probability for n and r_0/R is given by the product of probabilities of all q-space data points, as shown by Eq. (12), calculated for each measurement using Eq. (7) and repeated for all combinations of n and r_0/R to quantify the full 2D posterior probability distribution. The data shown here were simulated with $\langle\zeta\rangle = 2$ mm in the absence of self-diffusion and an outflow of spins. A ground truth of $n = 0.5$ and $r_0/R = 0.5$ was selected with SNR of 20 and 128 sampled q-space data points.

3. Materials and methods

3.1. Simulations

The sensitivity of the proposed Bayesian analysis approach to relevant experimental variables was investigated using numerical simulation experiments. All simulations were performed in MATLAB 2012b, operating under Windows 7. A modified version of Eq. (10) was used for the simulation of complex $S(q, n, r_0)$ data:

$$\frac{S(q, n, r_0)}{|S(0)|} = \int p'(\zeta, n, r_0) e^{i2\pi q\zeta - 4\pi^2 D(\Delta - \frac{\delta}{3})q^2} d\zeta + e(q), \quad (18)$$

where $e(q)$ represents the addition of pseudo-random Gaussian noise in quadrature, with zero mean and standard deviation σ. Using this approach, simulated $S(q, n, r_0)$ data were generated with the following parameters:

- The flow behaviour index was increased linearly between 0.1 and 1.0 in 10 steps.
- The radial position r_0/R, corresponding to τ_0/τ_w, was incremented linearly in 10 steps between 0.0 and 0.9, with R equal to 7 mm, consistent with that used experimentally.
- q-space was sampled linearly between $\pm q_{max}$, defined by the gradient timings and magnitude but approximately equal to $\pm 4\langle\zeta\rangle^{-1}$ m^{-1}, using 2^A points, with A taking integer values between 1 and 10 to sample 2–1024 points.
- Noise was incremented linearly between 0% and 10% in 11 steps, corresponding to SNR in the range 10–∞.

Note that, in all cases, SNR is defined as the ratio of the signal intensity at the centre of q-space to the standard deviation of the noise. The mean fluid displacement was 2 mm corresponding to an optimum q-space range of ± 2000 m^{-1}, as detailed in Section 2.

For Bayesian analysis of the simulated $S(q, n, r_0)$ data, and also that acquired experimentally, a simple uninformative prior ($p(\theta)$ in Eq. (6)) was used such that the probability of each of the parameter values considered was assumed to be identical. In particular, the range of priors comprised of a set of 501 values evenly spaced between 0 and 1 for both n and r_0/R, corresponding to a resolution of 0.002. Using the method outlined in Section 2, $f(q, n, r_0)$ was simulated for all n and r_0/R values and a 2D posterior probability distribution, $p(\theta|\hat{y})$, obtained; the means extracted from $p(\theta|\hat{y})$ provide an estimate of n and r_0/R, with the standard deviations a measure of the uncertainty. The numerical simulation experiments were repeated 100 times, each with pseudo-random Gaussian noise, for all combinations of parameters identified previously. Values reported in Section 4 correspond to the mean of the 100 means, with the standard deviation of the 100 means a measure of the uncertainty.

3.2. Experimental

3.2.1. Materials and experimental set-up

Aqueous solutions of Carbopol 940 (B.F. Goodrich, USA) were prepared in concentrations of 0.1 and 0.2 wt% using deionised water (ELGA Purelab Option). Complete dissolution of Carbopol 940 was achieved by stirring for 18 h using an overhead stirrer (Ika-Werke RW20); care was taken to prevent the entrapment of air during the stirring process. The pH was measured (Corning 240 pH meter) and adjusted to 4.5 and 5.0 for the 0.1 and 0.2 wt% Carbopol 940 solutions, respectively, using sodium hydroxide (Fisher Scientific, UK); these combinations of concentration and pH having previously been reported to demonstrate Herschel-Bulkley

rheological behaviour [30]. Although Carbopol 940 solutions are generally considered to exhibit little or no thixotropy [31], shear history-dependent behaviour at a Carbopol 940 concentration of ⩾0.2 wt% has previously been observed [7,8].

The flow system comprised a Perspex pipe of internal diameter (i.d.) 14 mm with a total loop volume of 1.5 L; the system was operated in a closed loop configuration. A peristaltic pump (MasterFlex Console Drive) capable of delivering flow rates of up to 50 mL s^{-1} was used, and steady flow was ensured through coupling of the pump with a flow pulsation dampener. Flow rates were determined gravimetrically. The radiofrequency (r.f.) coil was situated 1.5 m downstream of the pipe inlet, exceeding an inlet length of 60 times pipe i.d. which is recommended to ensure developed flow [41]. Pressure drop was measured across a length of 1.6 m using a differential pressure gauge (Digitron 2002P). For the 0.1 wt% Carbopol 940 solution, a pressure drop of 827 ± 41 Pa m^{-1} was measured at a flow rate of 16.3 ± 0.8 mL s^{-1}, where the uncertainty represents the standard deviation of five repeated measurements. A pressure drop of 3190 ± 190 Pa m^{-1} was measured for the 0.2 wt% Carbopol 940 solution at a flow rate of 3.00 ± 0.07 mL s^{-1}. These operating parameters correspond to a shear rate range of over two orders of magnitude; 0.1–63 and 0.1–22 s^{-1} for the 0.1 and 0.2 wt% Carbopol 940 solutions, respectively, as determined from MR flow imaging.

3.2.2. Magnetic resonance

All experiments were performed on a Bruker AV85 spectrometer operating with a 2 T horizontal-bore superconducting magnet. The magnet was fitted with a 60 mm i.d. birdcage r.f. coil tuned to a frequency of 85.2 MHz for the ^{1}H resonance. A three-axis gradient system with a maximum gradient strength of 10.7 G cm^{-1} was used for spatial and flow encoding.

A 13-interval alternating pulsed field gradient stimulated echo (APGSTE) pulse sequence was used, as shown in Fig. 5, to sample q-space data in the range of ±4⟨ζ⟩$^{-1}$ m^{-1} required for Bayesian analysis. Flow encoding gradients were applied with a duration (δ) and observation time (Δ) of 2 and 40 ms, respectively. The maximum gradient strength was 1.3 and 9.0 G cm^{-1} for the 0.1 and 0.2 wt% Carbopol 940 solutions, respectively, to sample q-space ranges of up to ±1080 and ±7660 m^{-1}. In both cases, q-space was sampled linearly in 128 steps (N). A total of 4 signal averages were acquired with a recycle time (TR) of 1.7 s, equal to 5 times T_1 (340 ms), giving a total data acquisition time of 15 min. This is equivalent to 7 s per data point acquired. Flow rates quantified through measurement of the evolution of the phase at low values of q, as described in Section 2, were 15.8 ± 0.5 and 3.16 ± 0.09 mL s^{-1} for the 0.1 and 0.2 wt% Carbopol 940 solutions,

respectively, in agreement with the gravimetric measurements to within the experimental uncertainty.

Volume-averaged flow propagators were also acquired to demonstrate the changes in flow distribution at the two Carbopol 940 concentrations studied using the same APSGTE pulse sequence that was used for the Bayesian NMR but with a different range of q-space data points. Flow encoding gradient timings and magnitudes were concentration specific. For the 0.1 wt% Carbopol 940 solution, δ = 3 ms and Δ = 60 ms with a maximum gradient strength of 2.3 G cm^{-1} to provide a FOF of 4⟨ζ⟩ mm, corresponding to a q-space range of up to ±2870 m^{-1}. For the 0.2 wt% Carbopol 940 solution, flow encoding gradients were applied with δ = 2 ms and a maximum gradient strength of 9.5 G cm^{-1}, with Δ = 100 ms. This corresponds to a q-space range of up to ±8090 m^{-1}. In both cases, N = 128 steps. A total of 4 signal averages were acquired with TR = 1.7 s, giving a total acquisition time of approximately 15 min.

In addition, spatially resolved velocity images were acquired for each Carbopol 940 solution investigated using a slice selective spin-echo MR flow imaging sequence [16], with a slice thickness of 10 mm. A field-of-view of 18 mm was selected in both the read and phase directions, with 128 phase increments and 128 read points, to give a resolution of 141 μm × 141 μm. Data were acquired such that the SNR within each liquid-filled voxel was 100. Flow encoding gradients were applied with δ = 2 ms and Δ = 10 ms, and δ = 2 ms and Δ = 40 ms, for the 0.1 and 0.2 wt% Carbopol 940 solutions, respectively. Two increments in g were utilised with the strength calibrated for each concentration to ensure a maximum phase shift of 2π. Images were acquired in 8 min with a recycle time of 450 ms and 4 signal averages. A non-linear least squares (NLLS) regression of the velocity (or displacement) image data to Eq. (4) was used to estimate rheological parameters n and r_0, with the 95% confidence interval in the individual fit a measure of uncertainty and the corresponding pressure drop data providing $τ_0$ and k. All NMR experiments were performed at 19.0 ± 0.5 °C. Flow rates calculated from the 2D velocity images were 15.8 ± 0.8 and 2.92 ± 0.15 mL s^{-1} for the 0.1 and 0.2 wt% Carbopol 940 solutions, respectively, in agreement with those obtained from the gravimetric measurements and low q-space analysis to within the experimental uncertainty.

3.2.3. Conventional rheometry

Benchtop measurements of the rheological properties of each Carbopol 940 solution investigated were performed using a Bohlin Instruments CVO-120 HR rheometer equipped with a Peltier plate to control the temperature to 19.0 ± 1.0 °C. The rheometer was operated in controlled-stress mode. In this mode of operation, the yield stress is obtained without the need for extrapolation, as is required when operating in controlled-rate mode [42]. A smooth-walled, 40 mm diameter parallel plate geometry was used with a plate separation of 0.75 mm; apparent shear rate was measured across a shear stress sweep of 0.01–100 Pa in 4 min. A correction is required to be applied to the apparent flow curve to obtain the true flow curve [42], given by:

$$\tau_a = \frac{4}{3}\tau_0 + \left(\frac{4}{3+n}\right)k\dot{\gamma}_a^n, \tag{19}$$

for the case of a parallel plate rheometer, where τ_a and $\dot{\gamma}_a$ represent the apparent (measured) shear stress and shear rate, respectively. The NLLS regression of Eq. (19) to the apparent flow curve, across the same shear rate ranges as probed in the Bayesian NMR and MR flow imaging experiments, was used to provide estimates of the rheological parameters. This regression is shown in Fig. 6 for the 0.1 and 0.2 wt% Carbopol 940 solutions, with the regression data within the scatter of the experimental data, confirming Herschel-Bulkley rheological behaviour over the shear rate ranges of the
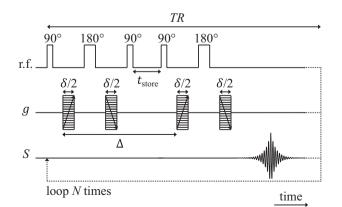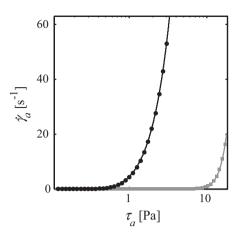

Fig. 5. Schematic of the 13-interval APGSTE sequence used for the acquisition of the volume-averaged flow propagator and data for Bayesian analysis.

Fig. 6. Apparent shear rate-shear stress data for the (●) 0.1 and (■) 0.2 wt% Carbopol 940 solutions obtained using conventional rheometry. The symbols show the experimentally acquired data and the solid lines show the regression data. Regression was performed over the shear rate range of the NMR experiments using Eq. (19).

Fig. 7. A 2D posterior probability distribution, plotted on a log scale, showing the probability of n and r_0/R given the experimental observations $\hat{y}$ obtained using simulated data. The data were generated with 128 sampled q-space data points and SNR of 100 for a ground truth of $n = 0.5$ and $r_0/R = 0.5$.

NMR experiments. The rheological parameters obtained across the range of shear rates investigated are summarised in Table 1, where the uncertainty represents the 95% confidence interval in the individual fit. An increase in concentration of Carbopol 940 from 0.1 to 0.2 wt% (and an increase in pH from 4.5 to 5.0) is responsible for a reduction in n, from 0.60 ± 0.02 to 0.28 ± 0.01. There is also an increase in both τ_0 and k, from 0.31 ± 0.01 to 3.3 ± 0.1 Pa and 0.22 ± 0.01 to 4.8 ± 0.1 Pa s^n, respectively, with these trends in agreement with literature values [30]. There was no evidence of wall slip in the data obtained.

4. Results and discussion

4.1. Numerical simulations: sensitivity to the Herschel-Bulkley parameters

The results of the numerical simulations described in Section 3.1 are now presented and discussed. A full 2D posterior probability distribution, $p(\theta|\hat{y})$, generated using simulated data with SNR of 100 and 128 sampled q-space data points is shown in Fig. 7. From $p(\theta|\hat{y})$, estimates of $n = 0.51 \pm 0.02$ and $r_0/R = 0.50 \pm 0.02$ were obtained, where the uncertainties represent the standard deviation of n and r_0/R, accurate to within <2% of the ground truth of $n = 0.50$ and $r_0/R = 0.50$. With reference to Fig. 4(e), an increase in noise is observed to cause a broadening of the posterior distribution and a decrease in maximum probability. The sensitivity to noise is investigated in Section 4.2.

Considering only the data corresponding to 16 sampled q-space data points with SNR of 100, we can investigate the sensitivity of the accuracy of the propo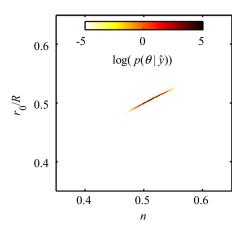sed Bayesian NMR approach to the estimation of the Herschel-Bulkley parameters. Fig. 8(a) shows the estimate of n, given by the mean of the 100 repeat simulation experiments, compared with the ground truth for three values of r_0/R. The accuracy of the estimate of n increases with an increase in r_0/R, however, the mean error in n remains <2% with a mean uncertainty (defined as the standard deviation of the 100 repeat simulation experiments) of 7%. Corresponding data for r_0/R for the three values of n reported in Fig. 8(b) show that the accuracy of the estimate of r_0/R is independent of the ground truth. Across the range of rheological parameters investigated, the mean error in r_0/R was <2% and the mean uncertainty was <7%. These results imply that the accuracy of the proposed Bayesian NMR approach is largely insensitive to changes in the rheological behaviour of the fluid under study, and therefore ideally suited to fluids demonstrating Herschel-Bulkley, power-law, and Newtonian rheology. Furthermore, only 16 points are required to be sampled in q-space with SNR of 100 if an accuracy of within 2% of the ground truth is acceptable for n and r_0/R, with an uncertainty of 7%.

4.2. Numerical simulations: sensitivity to noise and reduced sampling

As a technique, Bayesian analysis has previously demonstrated an excellent robustness to noisy data [32,37] and sparse sampling [33]. Here, this robustness was investigated for noise levels of up to 10%, corresponding to SNR of $\geqslant 10$, with as few as 2 sampled q-space data points. Fig. 9 shows the relationship between the estimate of n and the ground truth using simulated data with (a) 16 q-space data points and SNR of ∞, 100, and 50, and (b) a fixed SNR of 100 with 4, 16 and 64 q-space data points. For all cases, $r_0/R = 0.5$, with the estimate of n given by the mean of the 100 repeat simulation experiments.

Table 1

Comparison of the rheological parameters of the 0.1 and 0.2 wt% Carbopol 940 solutions obtained using conventional rheometry, MR flow imaging and Bayesian NMR methods. The parameters were evaluated across shear rate ranges of 0.1–63 and 0.1–22 s^{-1} for the 0.1 and 0.2 wt% Carbopol 940 solutions, respectively.

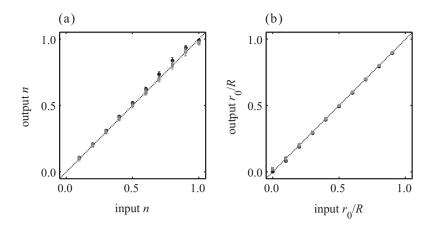| Concentration [wt%]	Method	Rheological parameters		
		n	τ_0 [Pa]	k [Pa s^n]
0.1	Conventional rheometry	0.60 ± 0.02	0.31 ± 0.01	0.22 ± 0.01
	MR flow imaging	0.55 ± 0.01	0.34 ± 0.04	0.25 ± 0.01
	Bayesian NMR	0.54 ± 0.01	0.32 ± 0.02	0.24 ± 0.01
0.2	Conventional rheometry	0.28 ± 0.01	3.3 ± 0.1	4.8 ± 0.1
	MR flow imaging	0.22 ± 0.01	3.4 ± 0.5	4.0 ± 0.1
	Bayesian NMR	0.30 ± 0.01	4.6 ± 0.1	2.4 ± 0.1

Fig. 8. (a) A comparison between the input n, i.e. ground truth, and output n, i.e. estimate, using the proposed Bayesian analysis approach with SNR of 100 and 16 sampled data points, plotted for r_0/R equal to (●) 0.0, (■) 0.2, and (▲) 0.5. (b) Corresponding data plotted for the estimate of r_0/R with n equal to (●) 1.0, (■) 0.8, and (▲) 0.5. Error bars represent the standard deviation of the 100 repeat simulation experiments, i.e. the uncertainty. The diagonal line (▪▪▪) represents the expected result, i.e. input = output.
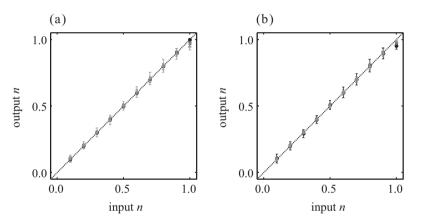

Fig. 9. (a) A comparison between the input n, i.e. ground truth, and output n, i.e. estimate, using the proposed Bayesian analysis approach with $r_0/R = 0.5$ and 16 sampled data points, with SNR equal to (●) ∞, (■) 100, and (▲) 50. (b) The same comparison using data with SNR of 100 and (●) 4, (■) 16, and (▲) 64 sampled data points. Error bars represent the standard deviation of the 100 repeat simulation experiments, i.e. the uncertainty. The diagonal line (▪▪▪) represents the expected result, i.e. input = output.

Fig. 9(a) shows that the accuracy of the estimation of n utilising 16 sampled q-space data points is insensitive to a reduction in SNR from ∞ to 50, with all results accurate to within <2% of the ground truth and absent of systematic error. As expected, the mean uncertainty associated with the estimation of n increases with a reduction in SNR, from 0% at an SNR of ∞ up to 9% at an SNR of 50. Despite the reduction in SNR, the accuracy of the estimation of n remains comparable to that of conventional rheometry techniques [9], suggesting that the proposed Bayesian NMR approach is robust to noisy data. If we now consider the number of sampled q-space data points, for a fixed SNR of 100, we observe in Fig. 9(b) that the accuracy of the estimation of n is increased as the number of sampled q-space data points is increased. For example, an increase in the number of sampled q-space data points from 4 to 64, representing a sixteen-fold increase in the experimental acquisition time, leads to a reduction in the mean error from 2% to <1%. The mean uncertainty across the same range decreases from 10% to <3%. Similar trends were observed for the estimation of r_0/R.

In summary, the proposed Bayesian NMR approach has demonstrated an excellent robustness to noisy data and reduced sampling. For an SNR of 100, only 16 q-space data points need to be sampled for accurate estimation of the rheological parameters. For cases where SNR > 100, this can be reduced further.

4.3. Experimental validation using NMR

4.3.1. Bayesian analysis

For validation of the results of the numerical simulations, Bayesian NMR experiments were performed on Carbopol 940 solutions demonstrating Herschel-Bulkley rheological behaviour. Fig. 10 shows the (a) real component and (b) imaginary component of the signal sampled at 128 points in q-space for the 0.1 and 0.2 wt% Carbopol 940 solutions. An increase in Carbopol 940 concentration from 0.1 to 0.2 wt% is observed to cause an increase in the magnitude of the signal at the limits of q-space sampled and a decrease in the frequency of the oscillations in q-space.

For completeness, we note that the changes observed in Fig. 10 are consistent with the volume-averaged flow propagators shown in Fig. 11, in which it is seen that an increase in concentration of Carbopol 940 is associated with a reduction in the maximum fluid displacement and an increase in the maximum probability (due to an increase in r_0/R). All flow propagators demonstrate a broadening due to self-diffusion and an absence of wall slip.

Methods outlined in Section 2 were used to obtain a 2D posterior probability distribution, $p(\theta|\hat{y})$, for each Carbopol 940 solution investigated, with the means and standard deviations of the distributions providing an estimate of n and τ_0 since $\mathrm{d}P/\mathrm{d}L$ was
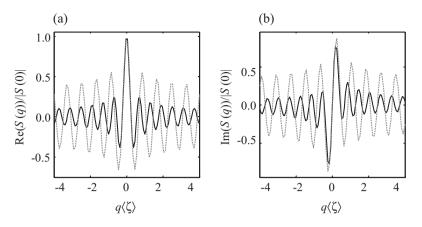
Fig. 10. Experimental results showing the evolution of the normalised (a) real and (b) imaginary components of the experimentally acquired $S(q)$, plotted across a q-space range of $\pm 4\langle\zeta\rangle^{-1}$ m^{-1} for the (—) 0.1 and (- -) 0.2 wt% Carbopol 940 solutions; SNR > 1000.
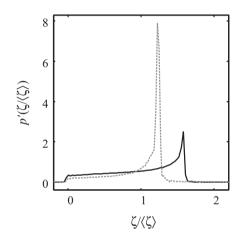

Fig. 11. Experimentally acquired flow propagators for the (—) 0.1 and (- -) 0.2 wt% Carbopol 940 solutions. Displacement is represented as a fraction of mean fluid displacement.

measured. The value of k was estimated using Eqs. (13)–(17) to enable recovery of the flow curve. Generated 2D posterior probability distributions for the 0.1 and 0.2 wt% Carbopol 940 solutions are shown in Fig. 12. For the 0.1 wt% Carbopol 940 solution, analysis of the posterior probability distribution provided n and τ_0 values of 0.54 ± 0.01 and 0.32 ± 0.02 Pa, respectively, with the uncertainties reported equal to the standard deviation of the distributions, and k estimated to equal 0.24 ± 0.01 Pa s^n. Rheological

parameters obtained for the 0.2 wt% Carbopol 940 solution using this approach are 0.30 ± 0.01, 4.6 ± 0.1 Pa, and 2.4 ± 0.1 Pa s^n for n, τ_0, and k, respectively.

The robustness to reduced sampling was investigated by the successive elimination of q-space data points between the maximum range of q-space sampled, with n and τ_0 values determined for each case. Fig. 13 shows the variation in the experimentally determined (a) n and (b) τ_0 for the 0.1 and 0.2 wt% Carbopol 940 solutions as the number of sampled q-space data points is reduced. The data show that n and τ_0 values obtained remain insensitive to the number of sampled q-space data points up to undersampling in excess of 80% (from 128 to 20 sampled q-space data points). Although there is a noticeable increase in error at a higher level of undersampling, Fig. 13 shows that a robust measurement of n (with an error of <5%) can be obtained when only 2 q-space data points are sampled, with up to 8 q-space data points required for the accurate estimation of τ_0. The acquisition of 8 q-space data points would correspond to a data acquisition time of <60 s, for four signal averages and a recycle time of 1.7 s, representing a reduction in acquisition time of 88% when compared with the acquisition of an MR flow image. Although a simple linear sampling scheme has been used here, it may be possible to further reduce the number of required q-space data points by choosing non-linear sampling schemes.

4.3.2. Comparison of Bayesian analysis with MR flow imaging and conventional rheometry approaches

The rheological parameters estimated using each of the Bayesian NMR, MR flow imaging and conventional rheometry methods
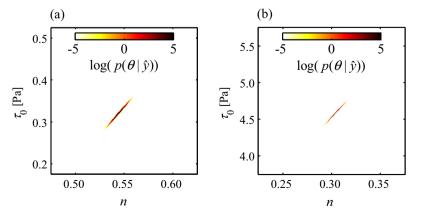

Fig. 12. 2D posterior probability distributions, plotted on a log scale, showing the probability of n and τ_0 given $\hat{y}$ for the (a) 0.1 and (b) 0.2 wt% Carbopol 940 solutions. The SNR (at $q = 0$ m^{-1}) is >1000, with the 128 points in q-space sampled using the experimental procedure outlined in Section 3.2.2.
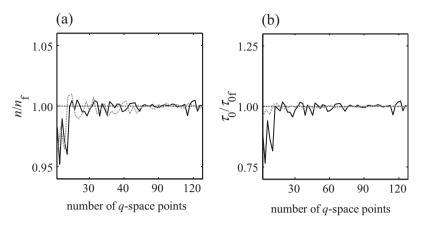
Fig. 13. Plots to demonstrate the relationship between the number of points sampled in q-space and (a) n and (b) τ_0 values obtained for the (━) 0.1 and (╍) 0.2 wt% Carbopol 940 solutions. For clarity, the n and τ_0 values are represented as a fraction of those parameters obtained using 128 sampled q-space data points (n_f and τ_{0f}, respectively). The horizontal line (┅) represents the ideal result.

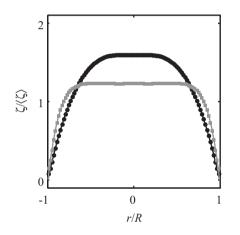**Fig. 14.** Displacement profiles, generated from radially-averaged 2D velocity image data, shown for the (●) 0.1 and (■) 0.2 wt% Carbopol 940 solutions, with fluid displacement and radial position represented as a fraction of the mean fluid displacement and pipe radius, respectively. The solid lines represent the radially-averaged 2D regression data, with the fitted data within the accuracy of the experimental data.

are summarised in Table 1. Before comparing these data, the results of the MR flow imaging method are presented.

Fig. 14 shows the radially-averaged 2D velocity image data obtained from the 2D z-velocity image acquired for each Carbopol

940 solution investigated. It is observed that the increase in concentration of Carbopol 940 from 0.1 to 0.2 wt% is responsible for a decrease in the maximum scaled displacement and an increase in r_0/R.

The 2D NLLS regression of $\Delta^{-1}\zeta(r)$ was performed to the 2D velocity image data for each Carbopol 940 solution investigated to quantify n and r_0/R, with $\zeta(r)$ given by Eq. (4). These fits to the data are also shown in Fig. 14; the displacement profiles and regression data are in agreement to within experimental error. From these, τ_0 and k can be estimated using Eqs. (2) and (3) and (13)–(17), respectively. For the 0.1 wt% Carbopol 940 solution, this approach provided n and τ_0 values of 0.55 ± 0.01 and 0.34 ± 0.04 Pa, respectively, where the uncertainty is equal to the 95% confidence interval in the individual fit, with $k = 0.25 \pm 0.01$ Pa s^n. Rheological parameters obtained for the 0.2 wt% Carbopol 940 solution using this approach are 0.22 ± 0.01, 3.4 ± 0.5 Pa, and 4.0 ± 0.1 Pa s^n for n, τ_0, and k, respectively.

Considering Table 1, we can now compare the results from the Bayesian NMR and MR flow imaging methods with conventional rheometry. Fig. 15 shows the corresponding flow curves for the (a) 0.1 and (b) 0.2 wt% Carbopol 940 solutions, calculated using Eq. (1) with the parameters reported in Table 1. From Table 1, it is clearly seen that the values of n, τ_0, and k determined for the 0.1 wt% Carbopol 940 solution using the three different methods are consistent, with the numerical values of the rheological parameters obtained from the two MR methods consistent to within
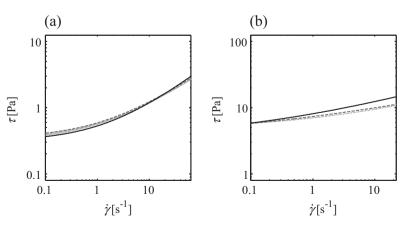

Fig. 15. Flow curves for the (a) 0.1 and (b) 0.2 wt% Carbopol 940 solutions obtained using (━) conventional rheometry, (╍) MR flow imaging, and (┅) Bayesian NMR, plotted across the shear rate ranges of the NMR experiments. The width of the line for the Bayesian NMR results represent the 95% confidence bands obtained from the 2D posterior probability distributions shown in Fig. 12.

experimental error. Furthermore, as shown in Fig. 15(a), the flow curves obtained from the three methods are almost identical. It is interesting to note that the 95% confidence bands shown in Fig. 15 for the Bayesian NMR results are small despite the uncertainty in the individual rheological parameters.

In contrast, with reference to Table 1, the rheological parameters determined for the 0.2 wt% Carbopol 940 solution using the three different methods show less good agreement. However, interestingly, despite the differences in values of the rheological parameters determined by the Bayesian NMR and MR flow imaging methods, their respective flow curves are almost indistinguishable from one another. This observation highlights the inability of the Herschel-Bulkley constitutive equation to unambiguously establish the rheological parameters, since different sets of these parameters can provide equivalent fits to the experimental data [4]. With reference to Fig. 15(b), it is seen that the flow curve determined using conventional rheometry is significantly different from those determined by the MR methods. This is most likely explained by the shear history-dependent behaviour of the 0.2 wt% Carbopol 940 solution, with differences of up to 40% in the yield stress of $\geqslant$0.2 wt% Carbopol 940 solutions previously reported [7,8], and the different flow geometries used. Since, in a process environment, the history-dependent behaviour of a process fluid is important, the ability of the Bayesian NMR approach to provide accurate measurements of rheological parameters online, or inline, and with acquisition times of <60 s is of great value.

5. Conclusions

A Bayesian NMR approach has been developed to enable the rheological characterisation of fluids demonstrating Herschel-Bulkley rheological behaviour in a pipe flow geometry using PFG NMR, requiring only single-axis gradient hardware. The approach utilises acquisition data directly, removing the need for Fourier transform, negating strict sampling requirements and hence permitting significant reductions in acquisition times.

An analytical expression describing the flow propagator in terms of rheological parameters appropriate to the Herschel-Bulkley constitutive equation was used, and a likelihood function developed to predict (or model) the PFG NMR signal for given n and r_0/R. This was used to obtain a posterior probability distribution through comparison with the experimentally acquired PFG NMR signal, enabling parameter estimation for n, with the pressure drop being used to estimate τ_0 and k. Simulation experiments performed indicated the proposed Bayesian NMR approach to be robust to noisy data and reduced sampling, with only 16 points required to be sampled in q-space at SNR of 100.

These numerical simulation studies were validated using experimentally acquired Bayesian NMR datasets for 0.1 and 0.2 wt% Carbopol 940 solutions. It was found that the Bayesian NMR approach provided estimates of the rheological parameters describing the Herschel-Bulkley fluids in <60 s. The estimates of the rheological parameters determined from Bayesian NMR were then compared with the same values determined using MR flow imaging and conventional rheometry. Whilst the rheological parameters, and hence flow curves, provided by all three methods for the 0.1 wt% Carbopol 940 solution were consistent, those for the 0.2 wt% Carbopol 940 solution were not. Both MR methods gave similar rheological characteristics but those measured from conventional rheometry differed significantly; this is most likely due to the shear history-dependent nature of the rheology of the 0.2 wt% Carbopol 940 solution and the different flow geometries used. The results presented therefore suggest that not only does the Bayesian NMR approach offer the convenience of fast data acquisition but that this may offer us new opportunities in the study and characterisation of history-dependent behaviour. We also note that the method is robust to relatively low signal-to-noise ratio and therefore offers opportunities for transfer to low and intermediate magnetic field hardware [43] for online, or inline, process monitoring.

Whilst this measurement has been demonstrated in application to Herschel-Bulkley fluids, it is readily applied to power-law fluids without further modification and can be easily adapted to other rheological models.

References

[1] P.C.F. Møller, J. Mewis, D. Bonn, Yield stress and thixotropy: on the difficulty of measuring yield stresses in practice, Soft Matter 2 (2006) 274–283.
[2] H.A. Barnes, K. Walters, The yield stress myth?, Rheol. Acta 24 (1985) 323–326.
[3] H.A. Barnes, The yield stress - a review or 'παντα ρει' - everything flows?, J. Non-Newton. Fluid Mech. 81 (1999) 133–178.
[4] R.M. Turian, T.W. Ma, F.L.G. Hsu, D.J. Sung, Characterization, settling, and rheology of concentrated fine particulate mineral slurries, Powder Technol. 93 (1997) 219–233.
[5] M. Benna, N. Kbir-Ariguib, A. Magnin, F. Bergaya, Effect of pH on rheological properties of purified sodium bentonite suspensions, J. Colloid Interf. Sci. 218 (1999) 442–455.
[6] A.A. Collyer, D.W. Clegg, Rheological Measurement, Springer, Netherlands, 1998.
[7] F. Caton, C. Baravian, Plastic behavior of some yield stress fluids: from creep to long-time yield, Rheol. Acta 47 (2008) 601–607.
[8] G. Benmouffok-Benbelkacem, F. Caton, C. Baravian, S. Skali-Lami, Non-linear viscoelasticity and temporal behavior of typical yield stress fluids: Carbopol, xanthan and ketchup, Rheol. Acta 49 (2010) 305–314.
[9] H.A. Barnes, J.F. Hutton, An Introduction to Rheology, Elsevier, Amsterdam, 1989.
[10] P.T. Callaghan, Rheo-NMR and velocity imaging, Curr. Opin. Colloid In. 11 (2006) 13–18.
[11] H.A. Barnes, A review of the slip (wall depletion) of polymer solutions, emulsions and particle suspensions in viscometers: its cause, character, and cure, J. Non-Newton. Fluid Mech. 56 (1995) 221–251.
[12] N.C. Shapley, R.A. Brown, R.C. Armstrong, Evaluation of particle migration models based on laser Doppler velocimetry measurements in concentrated suspensions, J. Rheol. 48 (2004) 255–279.
[13] S. Manneville, L. Bécu, A. Colin, High-frequency ultrasonic speckle velocimetry in sheared complex fluids, Eur. Phys. J. Appl. Phys. 28 (2004) 361–373.
[14] H.Y. Carr, E.M. Purcell, Effects of diffusion on free precession in nuclear magnetic resonance experiments, Phys. Rev. 94 (1954) 630–638.
[15] P.T. Callaghan, Principles of Nuclear Magnetic Resonance Microscopy, Clarendon Press, Oxford, 1993.
[16] L.F. Gladden, A.J. Sederman, Recent advances in flow MRI, J. Magn. Reson. 229 (2013) 2–11.
[17] D.F. Arola, G.A. Barrall, R.L. Powell, K.L. McCarthy, M.J. McCarthy, Use of nuclear magnetic resonance imaging as a viscometer for process monitoring, Chem. Eng. Sci. 52 (1997) 2049–2057.
[18] D.F. Arola, R.L. Powell, G.A. Barrall, M.J. McCarthy, A simplified method for accuracy estimation of nuclear magnetic resonant imaging, Rev. Sci. Instrum. 69 (1998) 3300–3307.
[19] D.F. Arola, R.L. Powell, G.A. Barrall, M.J. McCarthy, Pointwise observations for rheological characterization using nuclear magnetic resonance imaging, J. Rheol. 43 (1999) 9–30.
[20] A.J. Sederman, M.D. Mantle, C. Buckley, L.F. Gladden, MRI technique for measurement of velocity vectors, acceleration, and autocorrelation functions in turbulent flow, J. Magn. Reson. 166 (2004) 182–189.
[21] P. Galvosas, P.T. Callaghan, Fast magnetic resonance imaging and velocimetry for liquids under high flow rates, J. Magn. Reson. 181 (2006) 119–125.
[22] A.B. Tayler, D.J. Holland, A.J. Sederman, L.F. Gladden, Time resolved velocity measurements of unsteady systems using spiral imaging, J. Magn. Reson. 211 (2011) 1–10.
[23] J. Kärger, W. Heink, The propagator representation of molecular transport in microporous crystallites, J. Magn. Reson. 51 (1983) 1–7.
[24] J.E. Maneval, R.L. Powell, M.J. McCarthy, K.L. McCarthy, Magnetic Resonance Imaging of Multiphase Systems, Particulate and Two Phase Flow, Butterworth-Heinemann, Boston, 1993.

[25] E.O. Stejskal, J.E. Tanner, Spin diffusion measurements: spin echoes in the presence of a time-dependent field gradient, J. Chem. Phys. 42 (1965) 288–292.

[26] M.J. McCarthy, J.E. Maneval, R.L. Powell, Structure/Property Measurements Using Magnetic Resonance Spectroscopy and Imaging, Advances in Food Engineering, CRC Press, Florida, 1992.

[27] T.W. Blythe, A.J. Sederman, J. Mitchell, E.H. Stitt, A.P.E. York, L.F. Gladden, Characterising the rheology of non-Newtonian fluids using PFG-NMR and cumulant analysis, J. Magn. Reson. 255 (2015) 122–131.

[28] J.D. Seymour, J.E. Maneval, K.L. McCarthy, R.L. Powell, M.J. McCarthy, Rheological characterization of fluids using NMR velocity spectrum measurements, J. Texture Stud. 26 (1995) 89–101.

[29] G. Mullineux, Non-linear least squares fitting of coefficients in the Herschel-Bulkley model, Appl. Math. Model. 32 (2008) 2538–2551.

[30] F. Alberini, M.J.H. Simmons, A. Ingram, E.H. Stitt, Use of an areal distribution of mixing intensity to describe blending of non-Newtonian fluids in a Kenics KM static mixer using PLIF, AIChE J. 60 (2014) 332–342.

[31] Lubrizol Advanced Materials, Inc, Flow and Suspension Properties of Carbopol® Polymers, Technical Data Sheet (TDS-180), The Lubrizol Corporation, Ohio, 2002.

[32] G.L. Bretthorst, C.-C. Hung, D.A. d'Avignon, J.J.H. Ackerman, Bayesian analysis of time-domain magnetic resonance signals, J. Magn. Reson. 79 (1988) 369–376.

[33] D. Xing, S.J. Gibbs, J.A. Derbyshire, E.J. Fordham, T.A. Carpenter, L.D. Hall, Bayesian analysis for quantitative NMR flow and diffusion imaging, J. Magn. Reson. B 106 (1995) 1–9.

[34] R.G. Wise, B. Newling, A.R.C. Gates, D. Xing, T.A. Carpenter, L.D. Hall, Measurement of pulsatile flow using MRI and a Bayesian technique of probability analysis, Magn. Reson. Imag. 14 (1996) 173–185.

[35] G.L. Bretthorst, W.C. Hutton, J.R. Garbow, J.J.H. Ackerman, Exponential parameter estimation (in NMR) using Bayesian probability theory, Conc. Magn. Reson. A 27 (2005) 55–63.

[36] D.J. Holland, A. Blake, A.B. Tayler, A.J. Sederman, L.F. Gladden, A Bayesian approach to characterising multi-phase flows using magnetic resonance: application to bubble flows, J. Magn. Reson. 209 (2011) 83–87.

[37] J.G. Ross, D.J. Holland, A. Blake, A.J. Sederman, L.F. Gladden, Extending the use of earth's field NMR using Bayesian methodology: application to particle sizing, J. Magn. Reson. 222 (2012) 44–52.

[38] K. Ziovas, A.J. Sederman, C. Gehin-Delval, D.Z. Gunes, E. Hughes, M.D. Mantle, Rapid sphere sizing using a Bayesian analysis of reciprocal space imaging data, J. Colloid Interf. Sci. 462 (2016) 110–122.

[39] T. Chevalier, S. Rodts, C. Chevalier, P. Coussot, Quantitative exploitation of PFG NMR and MRI velocimetry data for the rheological study of yield stress fluid flows at macro- and micro-scales in complex geometries, Exp. Fluids 56 (2015) 1–16, Article No: 1868.

[40] R.A. Chilton, R. Stainsby, Pressure loss equations for laminar and turbulent non-Newtonian pipe flow, J. Hydraul. Eng. 124 (1998) 522–529.

[41] J.M. Coulson, J.F. Richardson, J.R. Backhurst, J.R. Harker, Coulson & Richardson's Chemical Engineering Volume 1: Fluid Flow, Heat Transfer, and Mass Transfer, Butterworth-Heinemann, Oxford, 1999.

[42] P.O. Brunn, H. Asoud, Analysis of shear rheometry of yield stress materials and apparent yield stress materials, Rheol. Acta 41 (2002) 524–531.

[43] J. Mitchell, T.C. Chandrasekera, D.J. Holland, L.F. Gladden, E.J. Fordham, Magnetic resonance imaging in laboratory petrophysical core analysis, Phys. Rep. 526 (2013) 165–225.